

# Comparison of HfO<sub>2</sub> films grown by atomic layer deposition using HfCl<sub>4</sub> and H<sub>2</sub>O or O<sub>3</sub> as the oxidant

Hong Bae Park, Moonju Cho, Jaehoo Park, Suk Woo Lee, and Cheol Seong Hwang<sup>a)</sup>  
*School of Materials Science and Engineering and Inter-university Semiconductor Research Center,  
Seoul National University, Seoul 151-742, Korea*

Jong-Pyo Kim, Jong-Ho Lee, Nae-In Lee, and Ho-Kyu Kang  
*System LSI, Semiconductor Business, Samsung Electronics Co., Ltd., Yong In Si 449-711, Korea*

Jong-Cheol Lee and Se-Jung Oh  
*School of Physics and Center for Strongly Correlated Materials Research, Seoul National University,  
Seoul 151-742, Korea*

(Received 3 April 2003; accepted 23 June 2003)

HfO<sub>2</sub> gate dielectric thin-films were deposited on Si wafers using an atomic-layer deposition (ALD) technique with HfCl<sub>4</sub> and either H<sub>2</sub>O or O<sub>3</sub> as the precursor and oxidant, respectively. Although the ALD reactions using either H<sub>2</sub>O or O<sub>3</sub> were successfully confirmed at a deposition temperature of 300 °C, the structural and electrical properties of the HfO<sub>2</sub> films grown using the two oxidants were quite different. The stronger oxidation power of the O<sub>3</sub> compared to H<sub>2</sub>O increased the oxygen concentration in the HfO<sub>2</sub> film and the rate of interfacial SiO<sub>2</sub> formation even at the as-deposited state. Because of the larger oxygen concentration, the decrease in the capacitance density of the film grown with O<sub>3</sub> after rapid thermal annealing at 750 °C under N<sub>2</sub> atmosphere was slightly larger than that of the HfO<sub>2</sub> film grown with H<sub>2</sub>O. Apart from this weakness, all the other electrical properties, including the fixed charge density, the interface trap density, the leakage current density and the hysteresis in the capacitance–voltage plot of the film grown with O<sub>3</sub> were superior to those of the film grown with H<sub>2</sub>O. Therefore, O<sub>3</sub> appears to be a better oxidant for the HfO<sub>2</sub> film growth using the ALD method. © 2003 American Institute of Physics. [DOI: 10.1063/1.1599980]

## I. INTRODUCTION

As complementary metal–oxide–semiconductor field effect transistor (CMOSFET) device scaling reaches the sub-0.1 μm era, high dielectric (high-*k*) HfO<sub>2</sub> thin films are attracting increasing interest as a replacement for nitrided SiO<sub>2</sub> gate oxide films.<sup>1–4</sup> Physically thicker high-*k* HfO<sub>2</sub> films can greatly suppress the gate leakage current ( $I_{\text{gate}}$ ) while maintaining a high gate capacitance. A high gate capacitance is essential in order to minimize the short-channel effect and to maximize the drain saturation current as well as to achieve the channel controllability of the gate.

The atomic layer deposition (ALD) process appears to be one of the most suitable methods for the high-*k* film growth due to its excellent process controllability even for extremely low thickness (<5 nm) high-*k* films.<sup>5,6</sup> However, most vapor-phase grown HfO<sub>2</sub> thin films appear to have interfacial layers (ILs) at the Si interface due to the presence of excess oxidizing elements, and simultaneous Si diffusion into the growing films.<sup>7,8</sup> This reduces the overall capacitance density, which needs to be minimized in order to realize the high-*k* characteristics. The other serious drawback of high-*k* gate oxides compared to SiO<sub>2</sub> is the high interfacial fixed-charge density ( $Q_f$ )<sup>9,10</sup> and the high interface trap density ( $D_{\text{it}}$ ).<sup>2,11</sup> The high  $Q_f$  and  $D_{\text{it}}$  adversely affect the device operation of the CMOSFET.

The commonly used precursor and oxidant for ALD of HfO<sub>2</sub> films are the HfCl<sub>4</sub> and H<sub>2</sub>O, respectively. This is because of the existence of a proper ligand exchange reaction between the two materials, which is inevitable for an ALD reaction to occur at a relatively low temperature (200–400 °C)<sup>8</sup> without thermal decomposition of the precursors. However, the HfO<sub>2</sub> films grown from the HfCl<sub>4</sub> contain a rather high concentration of Cl,<sup>12</sup> which might adversely affect the thermal stability and electrical performances of the film used as a gate dielectric. Lysaght *et al.*<sup>13</sup> recently reported that residual Cl ions in ALD HfO<sub>2</sub> films grown using HfCl<sub>4</sub> and H<sub>2</sub>O attack the underlying Si substrate and made voids in Si during postannealing, which is fatal to the MOSFET fabrication and operation. There might be some residual OH<sup>−</sup> and H<sup>+</sup> ions cracked from H<sub>2</sub>O in the film, which can also degrade the film properties.

O<sub>3</sub> has been used to grow high quality Al<sub>2</sub>O<sub>3</sub> films by the ALD using the Al(CH<sub>3</sub>)<sub>3</sub> as the Al precursor.<sup>14,15</sup> Compared to the Al<sub>2</sub>O<sub>3</sub> films grown by ALD using H<sub>2</sub>O as the oxidant, the films grown using O<sub>3</sub> appeared to have less incompletely oxidized Al ions,<sup>14</sup> thereby showing a better electrical performance, such as a smaller leakage current at a similar equivalent oxide thickness (EOT).<sup>15</sup> This can be attributed to the higher oxidizing power of O<sub>3</sub> compared to that of the H<sub>2</sub>O. Therefore, this study used O<sub>3</sub>, for the first time, for the ALD of HfO<sub>2</sub> films using the HfCl<sub>4</sub> precursor, and the growth behavior and structural and electrical proper-

<sup>a)</sup> Author to whom correspondence should be addressed; electronic mail: cheolsh@plaza.snu.ac.kr

ties of the films were compared to those of the films grown with the H<sub>2</sub>O oxidant.

## II. EXPERIMENTAL PROCEDURE

15–17-nm-thick HfO<sub>2</sub> films were grown by an ALD process using HfCl<sub>4</sub> and H<sub>2</sub>O or O<sub>3</sub> as the precursor and oxidant, respectively, at a wafer temperature of 300 °C on B-doped *p*-type 8-in.-diam (100) Si wafers (doping concentration of  $1 \times 10^{15} \text{ cm}^{-3}$ ). The native oxide on the Si wafer surface was removed by RCA cleaning immediately prior to HfO<sub>2</sub> film growth. Here, the film thickness was far larger than that used for the practical applications (3–4 nm). There are several reasons for such a large thickness. First was to measure the  $D_{it}$  using the conductance method, which requires a very low leakage current density ( $\sim 10^{-8} \text{ A cm}^{-2}$ ). It has been reported that single layer HfO<sub>2</sub> films with an EOT of 1–2 nm show a relatively large leakage ( $10^{-3}$ – $10^{-1} \text{ A cm}^{-2}$ ) in the voltage region of interest, which renders the application of conductance method impossible.<sup>16</sup> The thick film in this study suppresses the leakage current to sufficiently low levels in the voltage region of interest so that the  $D_{it}$  could be successfully measured using the conductance method. Second, the qualitative analysis of the structural variation of the film, such as x-ray diffraction (XRD) and high-resolution transmission electron microscopy (HRTEM) with the variation in the oxidants required a rather thick film. It has been reported that ALD HfO<sub>2</sub> films remain amorphous when the film thickness is small ( $< \sim 5 \text{ nm}$ ) irrespective of the deposition conditions.<sup>8</sup> The rather thick films in this study were crystallized even at the as-deposited state. Therefore, a comparison between the crystallization behaviors of the HfO<sub>2</sub> films grown with either the H<sub>2</sub>O or O<sub>3</sub> becomes feasible.

Postannealing of the samples was performed using a rapid thermal annealing (RTA) process at temperatures ranging from 700 to 900 °C for 60 s in a pure N<sub>2</sub> atmosphere.

The film thickness and crystalline structures were investigated by ellipsometry, HRTEM, and XRD. Ten HRTEM pictures were taken for each sample to compensate for the error in the film thickness measurements due to local variations. The chemical composition and binding status of the films were investigated by secondary-ion mass spectroscopy (SIMS) and x-ray photoelectron spectroscopy (XPS) using Mg *K*  $\alpha$  radiation with a photon energy 1253.6 eV. The overall energy resolution was approximately 1 eV. For XPS analysis, 2–3-nm-thick HfO<sub>2</sub> films were grown with the H<sub>2</sub>O and O<sub>3</sub> oxidants, respectively.

The metal–insulator–semiconductor capacitors (MIS-CAPs) were fabricated by depositing Pt top electrodes using an electron beam evaporation method through a shadow mask. The accurate electrode area of each measured capacitor was measured by optical microscopy. The backside of the wafer was HF cleaned with Al metallization being subsequently applied. The MIS CAP was annealed at 400 °C for 30 min under a 5% H<sub>2</sub>/95% N<sub>2</sub> atmosphere. A Hewlett–Packard 4194A impedance meter and a 4140B picoammeter were used for the capacitance–voltage ( $C$ – $V$ ) and the current density–voltage ( $J$ – $V$ ) measurements, respectively.

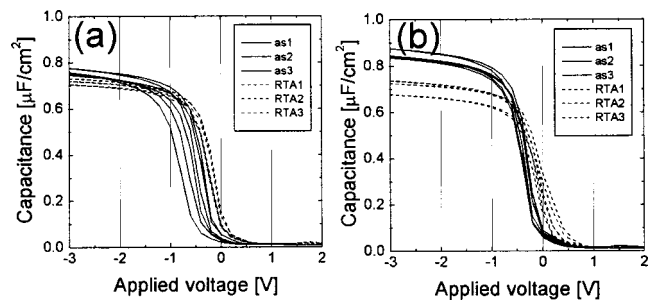


FIG. 1.  $C$ – $V$  curves of the MIS capacitor at the as-deposited state and after RTA at 750 °C of the HfO<sub>2</sub> film with (a) H<sub>2</sub>O and (b) O<sub>3</sub> as oxidants.

Five to ten capacitors were measured from each sample to compensate for local variations. The  $C$ – $V$  measurement frequency was 1 MHz. The conductance method was adopted to estimate the  $D_{it}$ .<sup>16</sup> Capacitance equivalent thickness (CET), flatband voltage shift ( $V_{fb}$ ), and hysteresis voltage ( $V_{hy}$ ) were extracted from the high-frequency  $C$ – $V$  curves.

## III. RESULTS AND DISCUSSION

Figures 1(a) and 1(b) show the  $C$ – $V$  curves of the MIS CAPs at the as-deposited state and after RTA at 750 °C of the HfO<sub>2</sub> film with the H<sub>2</sub>O and O<sub>3</sub> oxidants, respectively. The  $C$ – $V$  curves show a good saturation behavior due to the low leakage current, as shown in Fig. 2. Therefore, the CET was calculated from the accumulation capacitance (at  $-3 \text{ V}$ ). The variations in the CET values of the two HfO<sub>2</sub> films before and after postannealing are summarized in Table I along with the other electrical parameters as well as the thickness of each layer. First, the CET of the as-deposited HfO<sub>2</sub> film grown with O<sub>3</sub> shows a smaller CET by 0.5 nm than that of the film grown with H<sub>2</sub>O, which was due to the smaller thickness of the film as shown by the HRTEM in Fig. 4. However, the CETs of the films after RTA at 750 °C were almost the same indicating an inferior thermal stability of the HfO<sub>2</sub> film grown with the O<sub>3</sub> oxidant. This was attributed to the higher oxygen concentration of the film grown with the O<sub>3</sub> oxidant, as will be discussed later. Therefore, a fair comparison can be made by comparing the other electrical properties, such as the  $J$ ,  $V_{fb}$ ,  $V_{hy}$ , and  $D_{it}$ , of the two films after RTA.

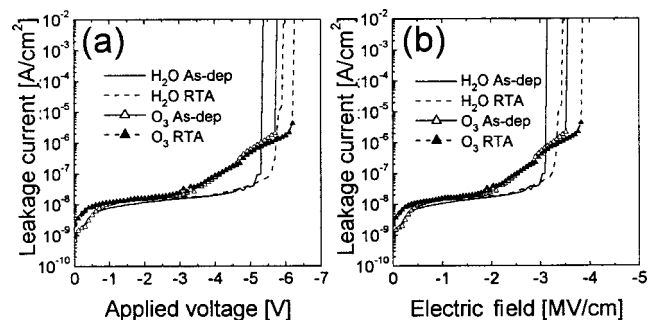


FIG. 2. (a)  $J$ – $V$  and (b)  $J$ – $E$  curves of the MIS capacitor at the as-deposited state and after RTA at 750 °C of the HfO<sub>2</sub> film grown with H<sub>2</sub>O and O<sub>3</sub> as oxidants.

TABLE I. Summary of the electrical results and the thickness variations.

Type of oxidant	Status	CET (nm) (-3 V)	Leakage (A/cm <sup>2</sup> ) (-1 V)	Hysteresis in C-V (mV)	Flatband voltage (mV)	Interlayer thickness (nm)	Upper-layer thickness (nm)	Total layer thickness (nm)
H <sub>2</sub> O	As-deposited	4.53	1.1 × 10 <sup>-8</sup>	161	-890	1.6	15.5	17.1
	RTA	4.80	1.4 × 10 <sup>-8</sup>	81	-520	1.4	15.8	17.2
O <sub>3</sub>	As-deposited	4.05	9.1 × 10 <sup>-9</sup>	92	-630	1.4	14.8	16.2
	RTA	4.85	1.0 × 10 <sup>-8</sup>	36	-300	1.7	14.5	16.2

The  $V_{fb}$  due to the fixed charges, which are assumed to be located at the interfacial layer/HfO<sub>2</sub> interface, were calculated by subtracting 0.6 V from the measured flatband voltage shift in the high frequency C-V curves in Fig. 1. Here the 0.6 V was the difference between the gate Pt work function [-5.6 eV for the (111) oriented Pt film] and Fermi level of the substrate Si. Figure 1 and Table I show that the HfO<sub>2</sub> film grown with O<sub>3</sub> has a smaller  $V_{fb}$  both at the as-deposited state and after RTA compared to that of the film grown with H<sub>2</sub>O at each state. The negative signs of all the measured  $V_{fb}$  values show that there are positive fixed charges irrespective of the type of oxidant used. The positive sign of the fixed charges at the HfO<sub>2</sub>/Si or HfO<sub>2</sub>/SiO<sub>2</sub> interfaces coincides very well with the theoretical estimation based on the bonding structure of the HfO<sub>2</sub><sup>17</sup> and recent experimental observations.<sup>18</sup> The smallest fixed charge density ( $Q_f$ ) observed for the case of the HfO<sub>2</sub> film grown with O<sub>3</sub> after RTA was still quite high ( $\sim 2.2 \times 10^{12} \text{ cm}^{-2}$ ) compared to the SiO<sub>2</sub>/Si interface. Here, the  $Q_f$  was calculated by multiplying the  $V_{fb}$  by capacitance density of the HfO<sub>2</sub> films. The capacitance densities of the HfO<sub>2</sub> films were calculated using the CET of HfO<sub>2</sub> layer, which was estimated by subtracting the interfacial layer CET from the measured CET. The interfacial layer CET was estimated from its physical thickness, observed by HRTEM, and the dielectric constants, which were assumed to be 6-7 and 4 for the as-deposited state and after RTA, respectively. Therefore, it is necessary to use a certain method to compensate for the positive fixed charge, such as adopting a thin Al<sub>2</sub>O<sub>3</sub> layer<sup>19</sup> or incorporating nitrogen into the high- $k$  film or interfacial layer for their practical application to MOSFET.<sup>20</sup>

The smaller  $V_{hy}$  measured from the voltage sweep from accumulation to inversion and back to accumulation shows that the HfO<sub>2</sub> film with the O<sub>3</sub> has a smaller density of slow interface states than that of the film grown with the H<sub>2</sub>O. The acceptable  $V_{hy}$  level (<50 mV) was obtained only from the HfO<sub>2</sub> film grown with O<sub>3</sub> after RTA. It should be noted that the thicker high- $k$  films usually show a larger  $V_{hy}$  due to the larger total number of slow state centers. Therefore, the  $V_{hy}$  of 36 mV is a very promising value considering the large thickness of the current single-layer HfO<sub>2</sub> film.

Figures 2(a) and 2(b) show  $J-V$  and  $J-E$  curves, respectively, of the MIS capacitor at the as-deposited state and after RTA at 750 °C of the HfO<sub>2</sub> film with the H<sub>2</sub>O and O<sub>3</sub> oxidants. Here, the electric field ( $E$ ) was the apparent electric field calculated by simply dividing the applied voltage by the total film thickness measured by HRTEM. The leakage current densities in the low voltage region (<-3 V) were very

low ( $< -5 \times 10^{-8} \text{ A/cm}^{-2}$ ), irrespective of the types of the oxidants and postannealing due to the thick thickness of the films. However, the  $J$  in the high voltage (>-3 V) region before breakdown was larger for the case of the films grown with O<sub>3</sub>. Interestingly, RTA does not change at all the  $J$  values irrespective of the types of the oxidants used but increases the breakdown field ( $E_{bd}$ ). The  $E_{bd}$  of the HfO<sub>2</sub> films with O<sub>3</sub> were larger than those of the films using H<sub>2</sub>O. The higher  $E_{bd}$ s of the as-deposited films and after RTA with the O<sub>3</sub> oxidant are believed to be due to the smaller surface roughness of the films as shown by atomic force microscopy (AFM) in Fig. 3. The rms roughness of the HfO<sub>2</sub> films grown with the H<sub>2</sub>O is 2-3 times larger than that of the films grown with the O<sub>3</sub> oxidant. The higher  $E_{bd}$  of the film after RTA with the O<sub>3</sub> oxidant compared to that of the as-deposited film is believed to be due to the larger interfacial layer thickness, which must have a higher resistivity, although the surface roughness slightly increased.

The fast increasing  $J$  after approximately -3 V prior to the breakdown of the film grown with O<sub>3</sub> might be related to the tunneling behavior due to the smaller thickness. Detailed analysis results for the leakage current mechanism of both samples will be reported in a later publication.

Figures 4(a)-4(d) show the HRTEM pictures of the as-deposited and RTA samples grown with the H<sub>2</sub>O and O<sub>3</sub> oxidants, respectively. The films appear to have partially crystallized structures at the as-deposited state and have better crystalline qualities after RTA. Although the comparison of the degree of crystallization of the samples using the HRTEM is not quantitative, the as-deposited film with the H<sub>2</sub>O

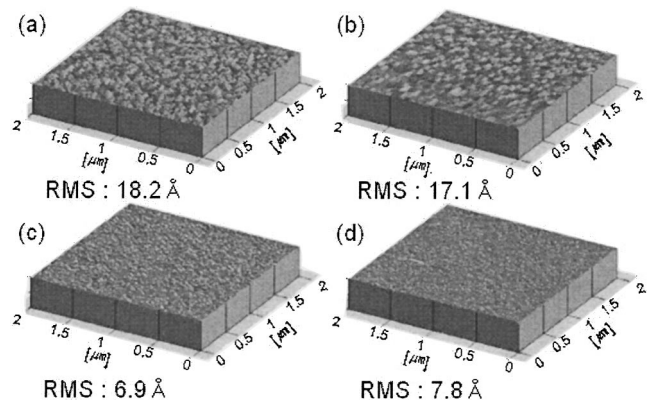


FIG. 3. AFM images of the (a) as-deposited sample grown with H<sub>2</sub>O, (b) RTA sample grown with H<sub>2</sub>O, (c) as-deposited sample grown with O<sub>3</sub>, and (d) RTA sample grown with O<sub>3</sub>.

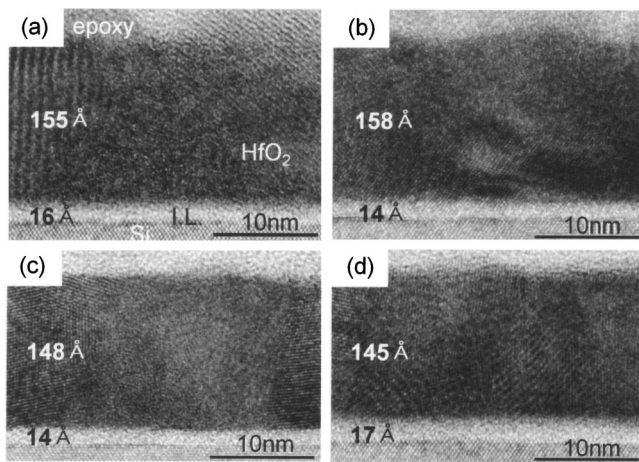


FIG. 4. HRTEM pictures of the (a) as-deposited sample grown with  $\text{H}_2\text{O}$ , (b) RTA sample grown with  $\text{H}_2\text{O}$ , (c) as-deposited sample grown with  $\text{O}_3$ , and (d) RTA sample grown with  $\text{O}_3$ .

oxidant appeared to have a relatively poor crystalline quality from the extensive HRTEM observations (more than ten HRTEM images). A more quantitative comparison between the crystalline qualities of the films was made using the XRD, as shown in Fig. 5. The films are composed of a thick  $\text{HfO}_2$  layer and thin interfacial layer. The thicknesses of each layer are included in Table I, where the thicknesses are the averaged values from ten HRTEM pictures of each sample. It has been reported that the thin  $\text{HfO}_2$  films ( $< \sim 5$  nm) grown directly on Si wafer at temperatures between 200 and 400 °C using the ALD method usually contain a rather high concentration of Si forming a Hf-rich Hf silicate.<sup>8</sup> The ILs contain some amount of Hf, particularly at the as-deposited state, forming a Si-rich Hf silicate.<sup>7</sup> However, the films in this study are rather thick and the surface regions (at least down to 10 nm depth from the surface) are almost completely free from Si impurities, as shown by the SIMS in Fig. 7. The IL thickness of the film grown with  $\text{H}_2\text{O}$  slightly decreases (by  $\sim 0.2$  nm) whereas that of the film grown with  $\text{O}_3$  slightly

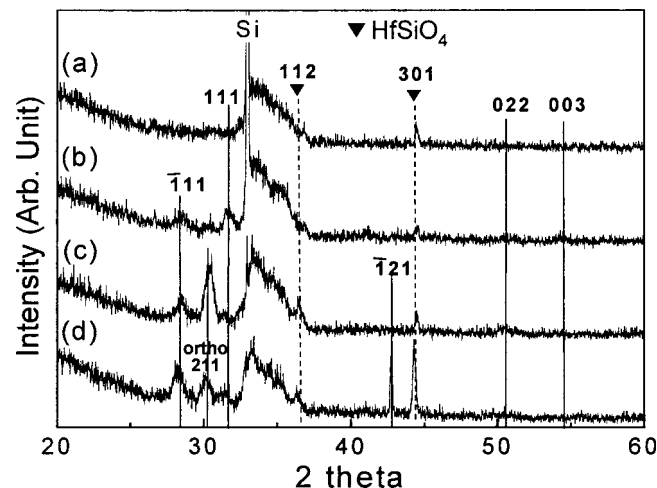


FIG. 5. XRD spectra of the (a) as-deposited sample grown with  $\text{H}_2\text{O}$ , (b) RTA sample grown with  $\text{H}_2\text{O}$ , (c) as-deposited sample grown with  $\text{O}_3$ , and (d) RTA sample grown with  $\text{O}_3$ .

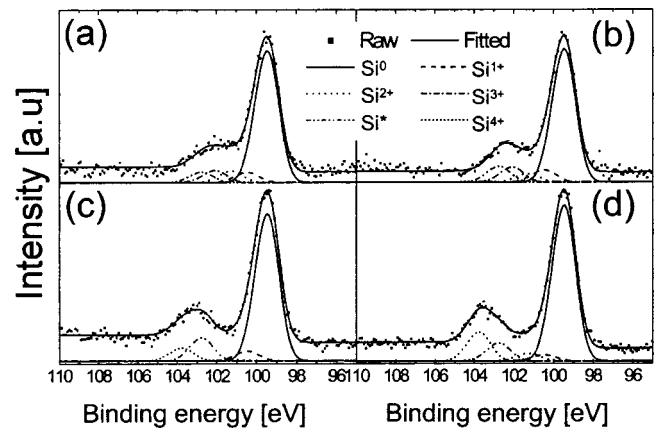


FIG. 6. Si  $2p$  XPS spectra of the (a) as-deposited sample grown with  $\text{H}_2\text{O}$ , (b) RTA sample grown with  $\text{H}_2\text{O}$ , (c) as-deposited sample grown with  $\text{O}_3$ , and (d) RTA sample grown with  $\text{O}_3$ .

increases (by  $\sim 0.3$  nm) after RTA. This increase in the IL thickness is due to oxidation of the Si substrate by the excess oxygen that was contained in the  $\text{HfO}_2$  film itself, and not by oxygen diffusion from the atmosphere. This can be confirmed by the XPS and SIMS results shown in Figs. 6 and 7, respectively.

Figure 5 shows the  $\theta$ - $2\theta$  XRD results of the samples before and after RTA at 750 °C. The as-grown film with the  $\text{H}_2\text{O}$  oxidant shows small peaks corresponding to crystalline  $\text{HfSiO}_4$  with no peaks corresponding to the  $\text{HfO}_2$ , although HRTEM showed the crystalline lattice fringes, which might be due to the small crystallite size of the  $\text{HfO}_2$  film. The presence of the  $\text{HfSiO}_4$  phase corresponds to the Si diffusion into the  $\text{HfO}_2$  film shown in the SIMS profile (Fig. 7). After RTA, peaks corresponding to the monoclinic  $\text{HfO}_2$  appear, suggesting the improvement in the crystalline quality or grain growth of the  $\text{HfO}_2$ , with a decrease in the intensity of the  $\text{HfSiO}_4$  peak. The as-grown film with  $\text{O}_3$  shows  $\text{HfO}_2$

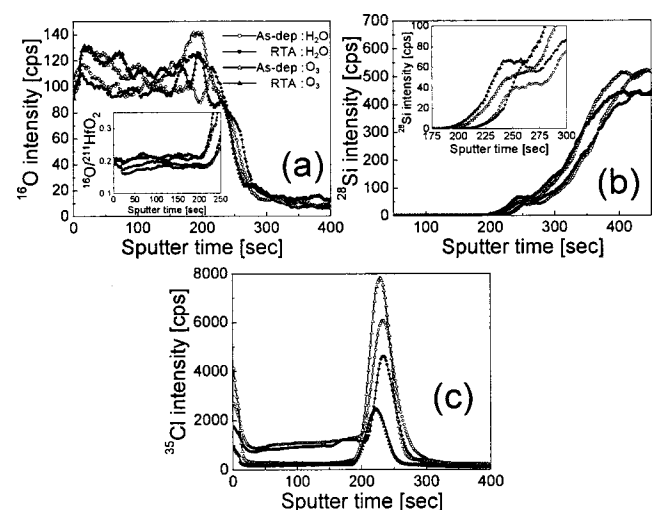


FIG. 7. SIMS depth profile results of (a) O (with mass 16) and (b) Si (with mass 28) of the thick  $\text{HfO}_2$  films grown with the  $\text{H}_2\text{O}$  and  $\text{O}_3$  before and after RTA at 750 °C. The inset (a) shows the variation in the O count/ $\text{HfO}_2$  (with mass 211) count ratio. The inset (b) shows the variation in the Si count near interface in detail. (c) Cl concentration profiles of the four samples.

peaks corresponding to the monoclinic and orthorhombic phases in addition to the  $\text{HfSiO}_4$  peaks. This suggests that the films grown with  $\text{O}_3$  are better crystallized compared to the films grown with  $\text{H}_2\text{O}$  although the growth temperatures were identical. Interestingly, RTA increases the  $\text{HfSiO}_4$  peak intensity in this case, whereas the films grown with the  $\text{H}_2\text{O}$  showed a lower  $\text{HfSiO}_4$  peak intensity after the same RTA, suggesting more Si-diffusion into the film occurred during RTA. This well corresponds to the Si concentration variation according to RTA estimated by the SIMS analysis shown in Fig. 7. RTA increased the Si concentration at the interface regions [see Fig. 7(b)]. RTA increases the monoclinic  $\text{HfO}_2$  peak intensities whereas the peak intensity corresponding to the orthorhombic  $\text{HfO}_2$  decreased. This is consistent with the fact that the monoclinic phase is the stable  $\text{HfO}_2$  phase at these temperatures.

The variations in the chemical composition and binding status of the  $\text{HfO}_2$  films with variations in the oxidants concentration ( $\text{H}_2\text{O}$  versus  $\text{O}_3$ ) and RTA were investigated by XPS. Since the 15–17-nm-thick  $\text{HfO}_2$  layer did not provide information on the interfaces, the  $\text{HfO}_2$  layer thickness was reduced to 2–3 nm for the XPS analysis. To more clearly observe the thermal treatment effect and to be more practical for the device fabrication, RTA temperature was increased to 950 °C for these thin samples. Figure 6 shows the Si 2*p* XPS spectra of the: (a) as-deposited sample grown with  $\text{H}_2\text{O}$ , (b) postannealed sample grown with  $\text{H}_2\text{O}$ , (c) as-deposited sample grown with  $\text{O}_3$ , and (d) postannealed sample grown with  $\text{O}_3$ . The spectra were deconvoluted assuming the presence of  $\text{Si}^0$  (Si substrate),  $\text{Si}^{1+}$ ,  $\text{Si}^{2+}$ ,  $\text{Si}^{3+}$ ,  $\text{Si}^*$  (Hf silicate), and  $\text{Si}^{4+}$  ( $\text{SiO}_2$ ) ions. The Si substrate peak was fixed at 99.3 eV. The variations in the  $\text{Si}^*$  and  $\text{Si}^{4+}$  peaks according to variation in the oxidant type during ALD and RTA should be noted. The as-deposited film grown with the  $\text{O}_3$  shows a rather strong  $\text{Si}^{4+}$  peak suggesting  $\text{SiO}_2$  formation at interface during film deposition. However, the as-deposited film grown with the  $\text{H}_2\text{O}$  shows no  $\text{Si}^{4+}$  peak suggesting that  $\text{SiO}_2$  was not formed at the interface during film deposition. Therefore, the ILs that were observed in the HRTEM of Fig. 4, comprised of  $\text{SiO}_2$ , Si suboxides and Si-rich Hf silicate for the case of the sample grown with the  $\text{O}_3$ , and merely Si suboxides and Si-rich Hf silicate for the case of the sample grown with the  $\text{H}_2\text{O}$ . This might be due to the higher oxidation potential of the  $\text{O}_3$  compared to that of the  $\text{H}_2\text{O}$ . It should be noted that there is almost no  $\text{Si}^{4+}$  signal detected for the case of the sample grown with the  $\text{H}_2\text{O}$  even after RTA. This clearly shows that there were barely any oxygen diffusion from the atmosphere and the formation of interfacial  $\text{SiO}_2$  during RTA at this temperature (950 °C) and time duration (1 min). In contrast, there is a certain increase in the  $\text{Si}^{4+}$  peak intensity after RTA for the case of the film grown with  $\text{O}_3$ . This suggests that oxygen, which is responsible for the interfacial  $\text{SiO}_2$  formation, was supplied from the  $\text{HfO}_2$  film itself grown with the  $\text{O}_3$ . This is consistent with the increase in the IL thickness by RTA observed by HRTEM only for the case of  $\text{O}_3$  in Fig. 4. The reason for the enhanced oxidation of the Si substrate during film growth and RTA can be found from the SIMS results.

Figures 7(a) and 7(b) shows the SIMS depth profile results of O (with mass 16) and Si (with mass 28), respectively, of the thick  $\text{HfO}_2$  films grown with the  $\text{H}_2\text{O}$  and  $\text{O}_3$  before and after RTA at 750 °C. The inset figure in (a) shows the variation in the O count/ $\text{HfO}_2$  (with mass 211) count ratio, which was included to more clearly show the higher concentration of oxygen for the case of the films grown with the  $\text{O}_3$  oxidant compared to the films grown with the  $\text{H}_2\text{O}$ . The longer sputter time of the film grown with  $\text{H}_2\text{O}$  to reach the Si substrate in both the O and Si profiling coincides with the thicker film shown by the HRTEM. It was difficult to detect any notable change in the O profile by RTA due to the rather small signal intensity of O. However, there is a notable change in the Si profiles particularly at the interface region by RTA, as shown in Fig. 7(b).

As discussed earlier, the surface region hardly has any Si impurities. The Si profiles at interface regions show plateaus in the sputter-etching time region of 250–275 s and 240–270 s for the as-deposited  $\text{HfO}_2$  films grown with the  $\text{H}_2\text{O}$  and  $\text{O}_3$  oxidants, respectively. These time span become narrower after RTA. These plateaus are believed to correspond to the ILs of each sample. Between the IL and bulk of the films, where no Si is detected, there is a transition layer with a Si diffusion profile. These regions are believed to be the Hf silicate, and their thicknesses were estimated to be approximately 3 and 4 nm for the as-deposited films grown with the  $\text{H}_2\text{O}$  and  $\text{O}_3$ , respectively, from their respective Si concentration transient time. This result coincides very well with the many reports regarding Hf-silicate formation for the cases of thin (<~5 nm)  $\text{HfO}_2$  film deposition by ALD and other methods.<sup>7,8,21</sup> The film grown with the  $\text{O}_3$  has a higher Si concentration both in the transition region and the IL before and after RTA compared to that of the film grown with  $\text{H}_2\text{O}$ . RTA increases the Si concentration in the IL by Si diffusion from the substrate for both cases. However, the Si concentration in the transition region of the film grown with  $\text{H}_2\text{O}$  does not increase at all whereas that of the film grown with  $\text{O}_3$  increases by RTA. This might be due to the higher oxygen concentration of the film grown with the  $\text{O}_3$ , i.e., excess oxygen in the  $\text{HfO}_2$  film offers an oxidation potential for the diffusing Si ions to form more Si–O bonds in the transition region (Hf silicate region). This increase in the Si concentration in the silicate region, in addition to the increase in the IL thickness, constitutes the reason for the larger increase in the CET by RTA for the case of the film grown using the  $\text{O}_3$  oxidant (see Table I and Fig. 1). The higher Si concentration in the transition region can also be confirmed by the Hf 4*f* XPS signal of the thin (2–3 nm) films shown in Fig. 8. Figure 7(c) shows the SIMS depth profile results of Cl concentration. It can be understood that the Cl concentrations of the films show peaks at the interface for each case. However, the Cl concentrations in the film bulk are far lower for the case of the films grown with the  $\text{O}_3$  oxidant compared to that of the film grown with the  $\text{H}_2\text{O}$ . RTA can greatly reduce the interfacial Cl contamination level but not the bulk Cl contamination. Therefore, using  $\text{O}_3$  as an oxidant was crucial to obtain a low Cl contamination level.

Figure 8 shows the Hf 4*f* XPS spectra of the (a) as-deposited sample grown with  $\text{H}_2\text{O}$ , (b) postannealed sample

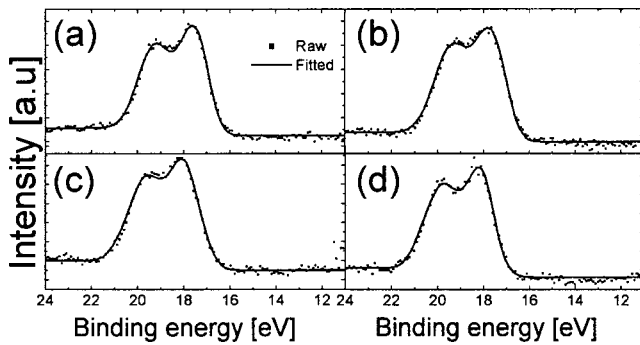


FIG. 8. Hf  $4f$  XPS spectra of the (a) as-deposited sample grown with  $\text{H}_2\text{O}$ , (b) RTA sample grown with  $\text{H}_2\text{O}$ , (c) as-deposited sample grown with  $\text{O}_3$ , and (d) RTA sample grown with  $\text{O}_3$ .

grown with  $\text{H}_2\text{O}$ , (c) as-deposited sample grown with  $\text{O}_3$ , and (d) postannealed sample grown with  $\text{O}_3$ . The Hf  $4f$  peak positions were calibrated using the Si substrate peak at 99.3 eV. The spectra were not deconvoluted. The rather high signal intensities in the binding energy region between the two Hf  $4f$  peaks by the spin-orbital splitting ( $4f_{7/2}$  and  $4f_{5/2}$ ) suggest that the films were composed of  $\text{HfO}_2$  and Hf silicate of which the Hf  $4f$  peak binding energies were located at higher values. From the comparison between the Hf  $4f$  peak positions from the as-deposited samples, it can be understood that these thin  $\text{HfO}_2$  films grown with  $\text{O}_3$  contains more Si compared to the film grown with  $\text{H}_2\text{O}$ . RTA at  $950^\circ\text{C}$  shifts the peak positions to a higher binding energy by approximately 0.1 and 0.2 eV for the cases of the films grown with  $\text{H}_2\text{O}$  and  $\text{O}_3$ , respectively. This qualitatively coincides with the SIMS results for the Si concentration variations of the transition regions in the thick films.

Figure 9 shows the variation in the  $D_{it}$  as a function of the trap energy ( $E_T$ )—the intrinsic Fermi energy ( $E_i$ ) of the various samples. The types of oxidants used during the growth primarily determine the  $D_{it}$ s of the samples. RTA at  $750^\circ\text{C}$  has little effect on the  $D_{it}$ . The films grown with  $\text{H}_2\text{O}$  showed a  $D_{it}$  level  $>10^{11}\text{ cm}^{-2}\text{ eV}^{-1}$ , whereas the films grown with  $\text{O}_3$  show mid- to low  $10^{10}\text{ cm}^{-2}\text{ eV}^{-1}$  near the

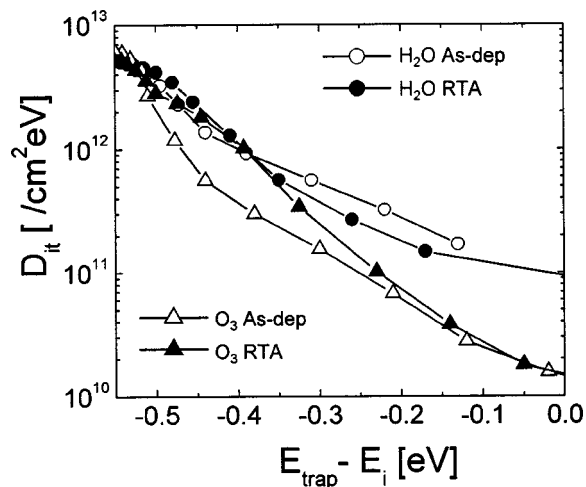


FIG. 9. Variation in the  $D_{it}$  as a function of the trap energy ( $E_T$ )—intrinsic Fermi energy ( $E_i$ ) of the various samples.

mid gap. This low  $D_{it}$  level is close to that of the  $\text{SiO}_2/\text{Si}$  interface. Considering  $\text{SiO}_2$  formation at the interface with Si for the case of the films grown with  $\text{O}_3$ , the small  $D_{it}$  is reasonable. This is a very important result since the high- $k/\text{Si}$  interface almost always suffers from a high  $D_{it}$ .<sup>2,11</sup>

#### IV. CONCLUSIONS

$\text{HfO}_2$  gate dielectric thin films were deposited on Si wafers by an ALD method using  $\text{HfCl}_4$  and either  $\text{H}_2\text{O}$  or  $\text{O}_3$  as the precursor and oxidant, respectively. The stronger oxidation power of the  $\text{O}_3$  compared to the  $\text{H}_2\text{O}$  increased the oxygen concentration in the  $\text{HfO}_2$  film and interfacial  $\text{SiO}_2$  formation, even at the as-deposited state. Because of the larger oxygen concentration, rapid thermal annealing at  $750^\circ\text{C}$  under  $\text{N}_2$  atmosphere produced a larger  $\text{SiO}_2$  formation at the interface and Hf silicate formation than that of the  $\text{HfO}_2$  film grown with  $\text{H}_2\text{O}$  oxidant. This results in a larger increase in the CET values compared to the  $\text{HfO}_2$  film grown with the  $\text{H}_2\text{O}$  oxidant. Apart from this weakness, all the other electrical properties, including the fixed charge density, interface trap density, leakage current density, and hysteresis in the capacitance–voltage plot, of the film grown with  $\text{O}_3$  were superior to those of the film grown with  $\text{H}_2\text{O}$ . In particular, the  $\text{HfO}_2$  films grown with  $\text{O}_3$  show a  $D_{it}$  level comparable to that of  $\text{SiO}_2/\text{Si}$  due to the presence of the interfacial  $\text{SiO}_2$ . Therefore,  $\text{O}_3$  appears to be a better oxidant for the  $\text{HfO}_2$  film growth using the ALD method considering both MOSFET and capacitor applications in memory devices.

#### ACKNOWLEDGMENTS

The work was supported by Korea Research Foundation (Grant No. KRF-2002-042-D00348), and Korea Ministry of Science and Technology through National Research Laboratories Program and National R&D Project for Nano Science and Technology (Grant No. M10214000097-02B1500-01500). S.-J. Oh acknowledges CSCMR and BK21 Program of Seoul National University.

<sup>1</sup>L. F. Schneemeyer, R. B. van Dover, and R. M. Fleming, Appl. Phys. Lett. **75**, 1967 (1999).

<sup>2</sup>G. D. Wilk, R. M. Wallace, and J. M. Anthony, J. Appl. Phys. **89**, 5243 (2001).

<sup>3</sup>W. Zhu, T. P. Ma, T. Tamagawa, Y. Di, J. Kim, R. Carruthers, M. Gibson, and T. Furukawa, Tech. Dig. Int. Electron Devices Meet. 463 (2001).

<sup>4</sup>H.-J. Cho, C. S. Kang, K. Onishi, S. Gopalan, R. Nieh, R. Choi, E. Dharmarajan, and J. C. Lee, Tech. Dig. Int. Electron Devices Meet. 655 (2001).

<sup>5</sup>P. M. Zeitzoff, R. W. Murto, and H. R. Huff, Solid State Technol. **45**, 71 (2002).

<sup>6</sup>A. Nakajima, T. Kidera, H. Ishii, and S. Yokoyama, Appl. Phys. Lett. **81**, 2824 (2002).

<sup>7</sup>B. K. Park, J. Park, M. Cho, C. S. Hwang, K. Oh, Y. Han, and D. Y. Yang, Appl. Phys. Lett. **80**, 2368 (2002).

<sup>8</sup>M. Cho, J. Park, H. B. Park, C. S. Hwang, J. Jeong, and K. S. Hyun, Appl. Phys. Lett. **81**, 334 (2002).

<sup>9</sup>R. S. Johnson, G. Lucovski, and I. Baumvol, J. Vac. Sci. Technol. A **19**, 1353 (2001).

<sup>10</sup>D.-G. Park, H.-J. Cho, K.-Y. Lim, C. Lim, I.-S. Yeo, J.-S. Roh, and J. W. Park, J. Appl. Phys. **89**, 6275 (2001).

<sup>11</sup>I. S. Jeon, J. Park, D. Eom, C. S. Hwang, H. J. Kim, C. J. Park, H. Y. Cho, J.-H. Lee, N.-I. Lee, and H.-K. Kang, Appl. Phys. Lett. **82**, 1066 (2003).

<sup>12</sup>M. Cho, J. Park, H. B. Park, C. S. Hwang, J. Jeong, K. S. Hyun, Y. W. Kim, C. Oh, and H. S. Kang, Appl. Phys. Lett. **81**, 3630 (2002).

<sup>13</sup>P. S. Lasaght, B. Fordan, G. Bersuker, P. J. Chen, R. W. Murto, and H. R. Huff, Appl. Phys. Lett. **82**, 1266 (2003).

- <sup>14</sup>J. B. Kim, D. R. Kwon, K. Chakrabarti, and C. Lee, *J. Appl. Phys.* **92**, 6739 (2002).
- <sup>15</sup>K. H. Hwang, S. J. Choi, J. D. Lee, Y. S. You, Y. K. Kim, H. S. Kim, C. L. Song, and S. I. Lee, ALD Symposium, Monterey, CA, 14 May 2001.
- <sup>16</sup>E. M. Vogel, W. K. Henson, C. A. Richter, and J. S. Suehle, *IEEE Trans. Electron Devices* **47**, 601 (2000).
- <sup>17</sup>R. S. Johnson, J. G. Hong, C. Hinkle, and G. Lucovski, *J. Vac. Sci. Technol. B* **20**, 1126 (2002).
- <sup>18</sup>B. Crivelli *et al.*, Presented at the Symposium Materials Research of the Society, Boston, MA, December 2–6, 2002.
- <sup>19</sup>M. Cho, H. B. Park, J. Park, C. S. Hwang, J. C. Lee, S. J. Oh, J. Jeong, and K. S. Hyun, *J. Appl. Phys.* **94**, 2563 (2003).
- <sup>20</sup>H. B. Park, M. Cho, J. Park, C. S. Hwang, J. C. Lee, and S. J. Oh, *J. Appl. Phys.* **94**, 1898 (2003).
- <sup>21</sup>M.-H. Cho, Y. S. Roh, C. N. Whang, K. Jeong, S. W. Nahm, D.-H. Ko, J. H. Lee, N. I. Lee, and K. Fujihara, *Appl. Phys. Lett.* **81**, 472 (2002).